OMTO, Volume *31*

Supplemental information

Improved oncolytic activity of a reovirus mutant that displays enhanced virus spread due to reduced cell attachment

Francisca Cristi, Maiah Walters, Nashae Narayan, Kate Agopsowicz, Mary M. Hitt, and Maya Shmulevitz

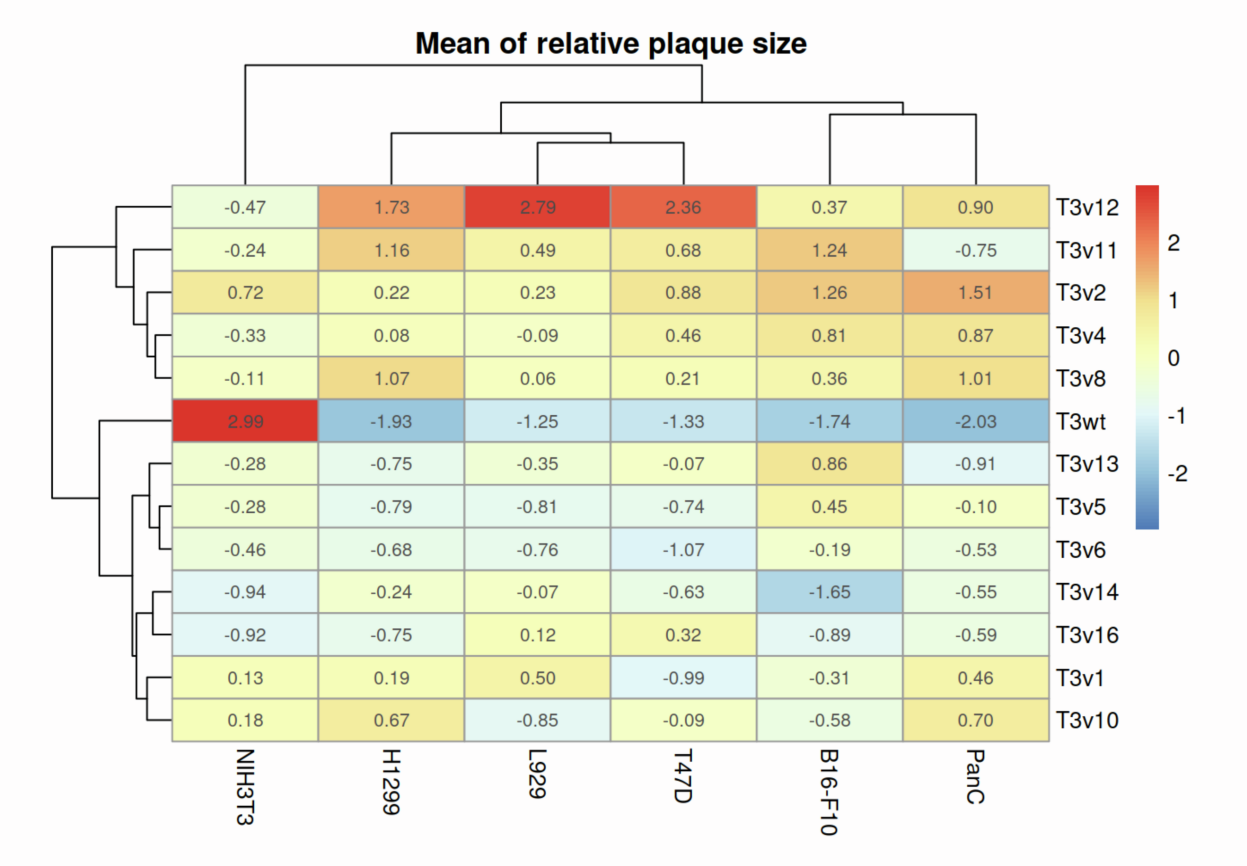

Figure S1: Heat map showing the differences in plaque size among the isolated reovirus mutants. The non-transformed cell line NIH3T3, as well as murine transformed L929 and B16-F10 cells and human transformed H1299, T47D, and PanC cells were infected with T3wt and mutants T3v1, T3v2, T3v4, T3v5, T3v6, T3v8, T3v10, T3v11, T3v12, T3v13, and T3v16. Cells were fixed and stained with crystal violet or subjected to IHC after 5-8 days of infection. The heat map shows the mean relative plaque size to T3wt for each isolated mutant and then scaled for each cell line (with the formula: (value - mean) / standard deviation). A higher number means that the mutant produces larger plaques than T3wt compared to the other mutants.

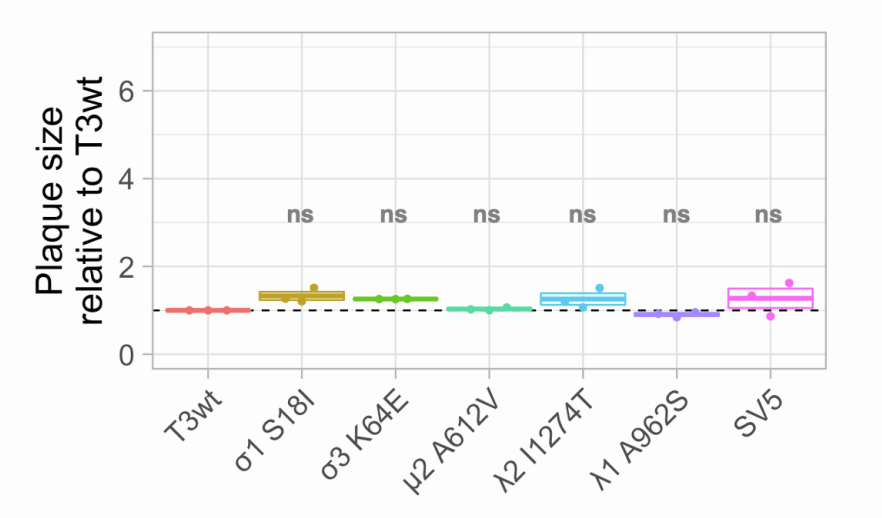

Figure S2: Oncolytic mutants do not produce larger plaques than T3wt in non-transformed BJ cells. Graph shows plaque size of the single-mutated viruses and SV5 relative to T3wt. Each point represents an individual experiment (n = 3). BJ cells (human fibroblasts from foreskin) were infected with T3wt, the single-mutated viruses σ1 S18I, σ3 K64E, μ2 A612V, λ2 I1274T or λ1 A962S, or the combined mutant SV5. Cells were fixed at 5 days post-infection. Immunocytochemistry using a polyclonal anti-reovirus antibody was performed to detect plaques.

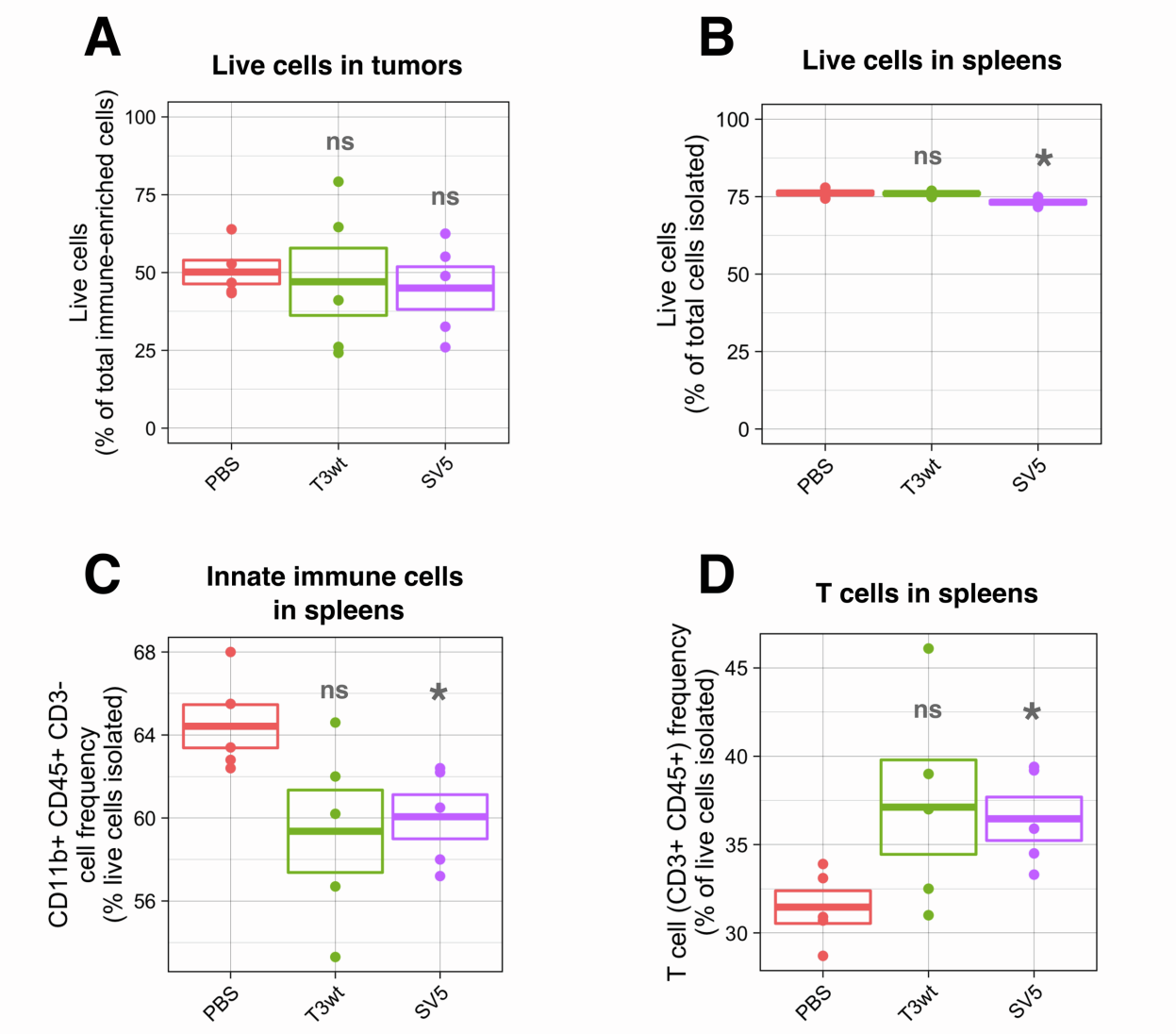

Figure S3: Frequency of live cells in spleens and tumors and frequency of innate immune cells and T cells in spleens after oncolytic treatment. Diagram of the animal experiment can be found in Figure 5A. TUBO cells were implanted into the mammary fat pad of BALB/c mice. When tumors were palpable, we performed three intratumoral injections (days 1, 3 and 5) with PBS or virus at 5 x 10^8 PFU/injection. At day 14 post-virus-injections mice were euthanized, and tumors and spleens were collected. Tumors samples were enriched for immune cells by Percoll gradient prior to flow cytometric analyses. **A.** Live immune-enriched cells (Zombie aqua- from total singlet cells) in tumors. **B.** Live cells (Zombie aqua- from total singlet cells) in spleen. **C.** Frequency of CD11b+/CD45+/CD3- cells in live cells in spleens. **D.** Frequency of T-lymphocytes (CD3+/CD45+) in live cells in spleens. n = 5 per group. *p<0.05, ns: non-significant. p-values were calculated with an ANOVA with Tukey test.

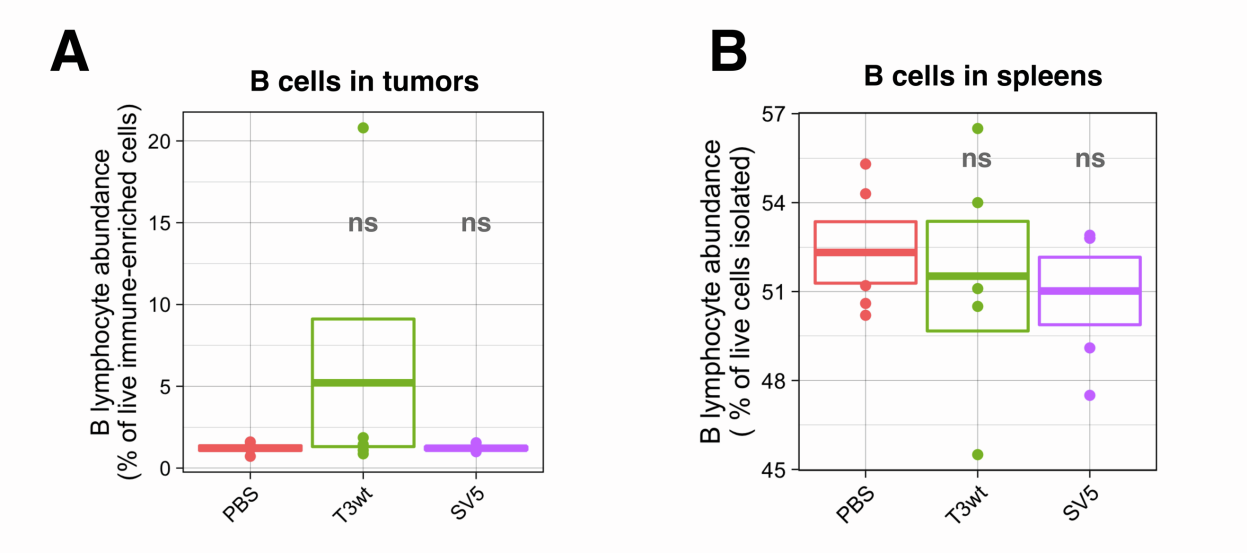

Figure S4: B lymphocyte abundance in tumors and spleens after oncolytic treatment. Diagram of the animal experiment can be found in Figure 5A. TUBO cells were implanted into the mammary fat pad of BALB/c mice. When tumors were palpable, we performed three intratumoral injections (days 1, 3 and 5) with PBS or virus at 5 x 10^8 PFU/injection. At day 14 post-first-virus injections mice were euthanized, and tumors (panel **A**) and spleens (panel **B**) were collected for immune analyses. Tumor samples were enriched for immune cells by Percoll gradient prior to flow cytometry. n = 5 per group. B cells were identified and graphed as a percentage of CD45+/CD19+ cells from live immune-enriched cells in the case of tumors and from live cells in the case of the spleens. P-values were calculated with an ANOVA with Tukey test, ns: non-significant.

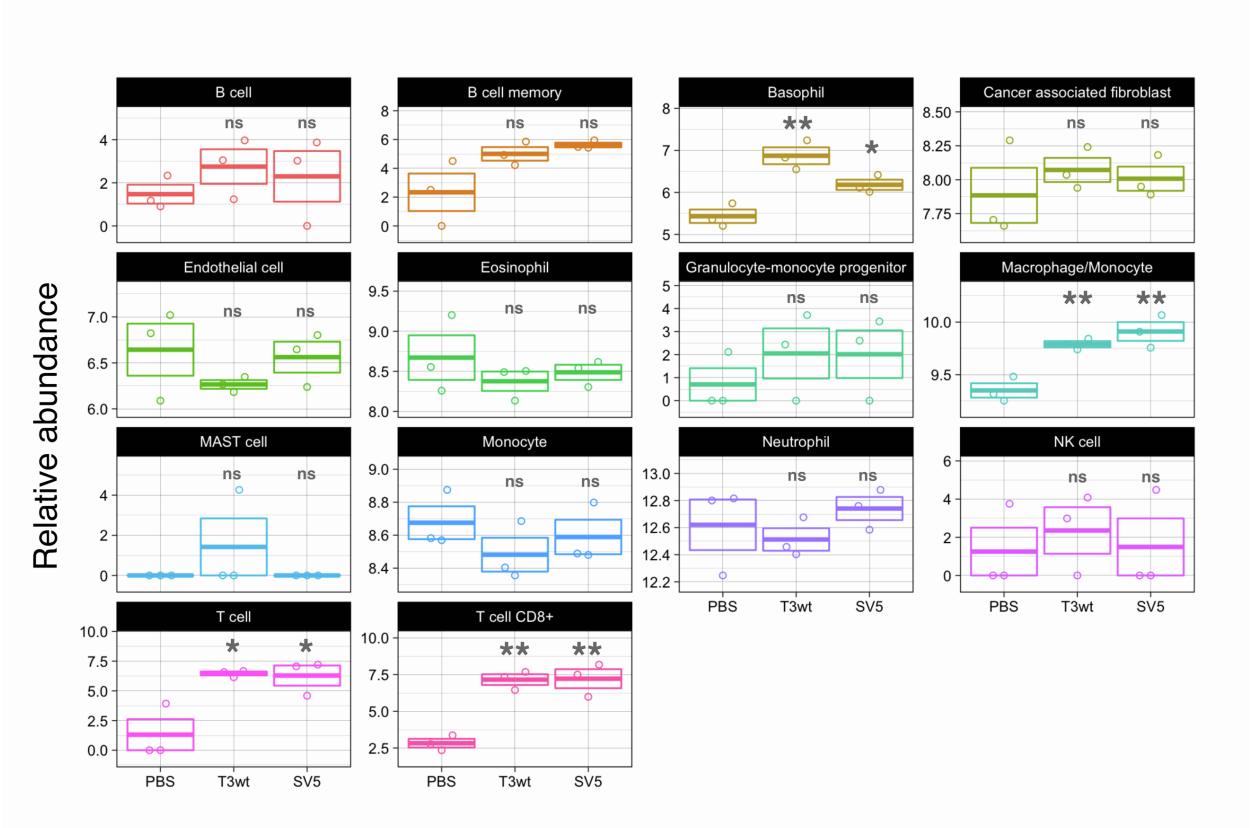

Figure S5: Abundance of tumor microenvironment cell populations in TUBO tumors after oncolytic treatment detected by RNA sequencing. Diagram of the experiment can be found in Figure 5A. TUBO cells were implanted into the mammary fat pad of BALB/c mice. When tumors were palpable, we performed 3 intratumoral injections (days 1, 3 and 5) with PBS or viruses at 5 x 10^8 PFU/injection. At day 14 post-first-virus injections, mice were euthanized, and tumors were collected for RNA sequencing. Three mice per group. The murine Microenvironment Cell Populations-counter (mMCP-counter) method and the Immunedeconv R package [1-3] were used to determine the frequency of immune cells in tumors following RNA sequencing. List of signatures genes used as transcriptomic markers can be found in the **Table S5** (modified Petitprez et al. 2020) [3]. *p<0.05, **p<0.01, ns: non-significant relative to PBS. p-values calculated with an ANOVA with Tukey test.

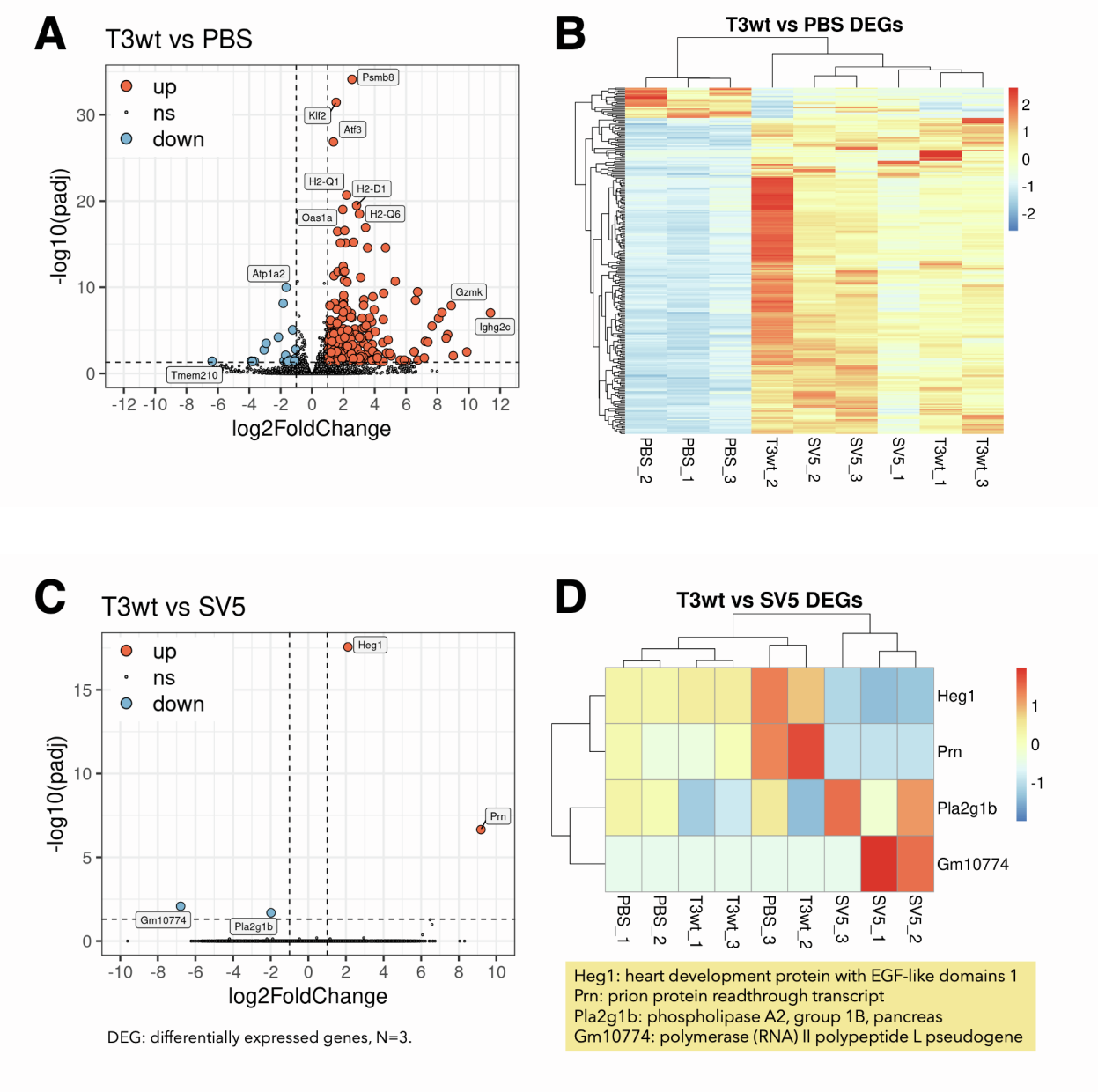

Figure S6: Only four genes are differentially expressed between T3wt- and SV5-treated TUBO tumors. Diagram of the animal experiment can be found in Figure 5A. TUBO cells were implanted into the mammary fat pad of BALB/c mice. When tumors were palpable, we performed three intratumoral injections (days 1, 3 and 5) with PBS or virus at 5 x 10^8 PFU/injection. At day 14 post-first-virus injections mice were euthanized, and tumors and spleens from three mice per treatment were collected for RNAseq analyses. **A.** Differential expressed genes in T3wt-treated tumors relative to PBS-treated tumors. Upregulated transcripts are shown in green and downregulated transcripts are shown in red. **B.** All differentially expressed genes between T3wt and PBS treatments shown as a heat map. Tumor samples are grouped by similarity in expression of the differentially expressed genes. Upregulated transcripts are shown in a red scale of colors and downregulated

transcripts are shown in a blue scale of colors. **C.** Differential expressed genes in T3wt-treated tumors relative to SV5-treated tumors. Upregulated transcripts are shown in green and downregulated transcripts are shown in pink. **D.** All differentially expressed genes between T3wt and SV5 treatments shown as a heat map. Tumor samples are grouped by similarity in expression of the differentially expressed genes. Upregulated transcripts are shown in a red scale of colors and downregulated transcripts are shown in a blue scale of colors.

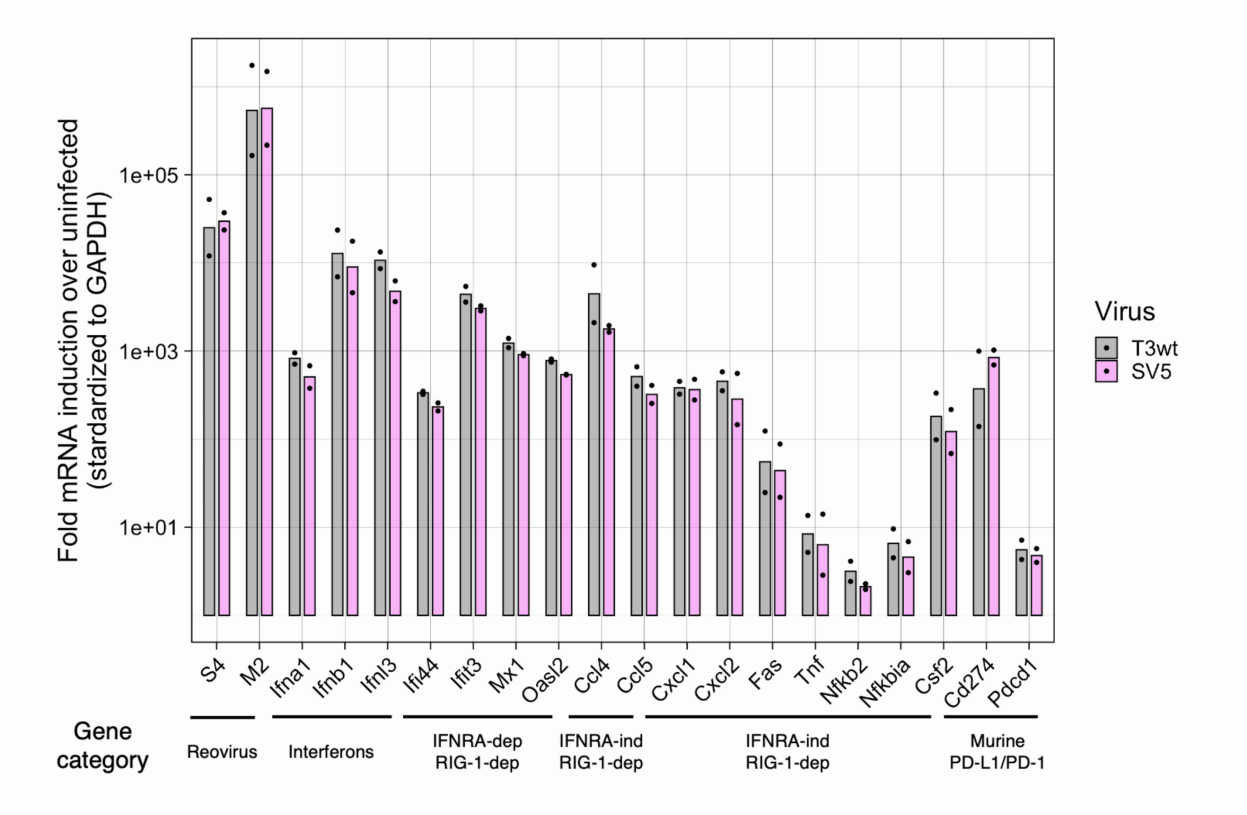

Figure S7: SV5 does not induce a different expression profile than T3wt in TUBO cells. TUBO cells were infected with either T3wt or SV5 at an MOI to get equal infected cells after 15 hpi, evaluated by immunofluorescence. RNA was extracted and qRT-PCR to detect mRNA levels of viral and immune genes was done (n = 2). Genes corresponding to the different pathways were obtained from Mohamed et. al. 2020 [4].

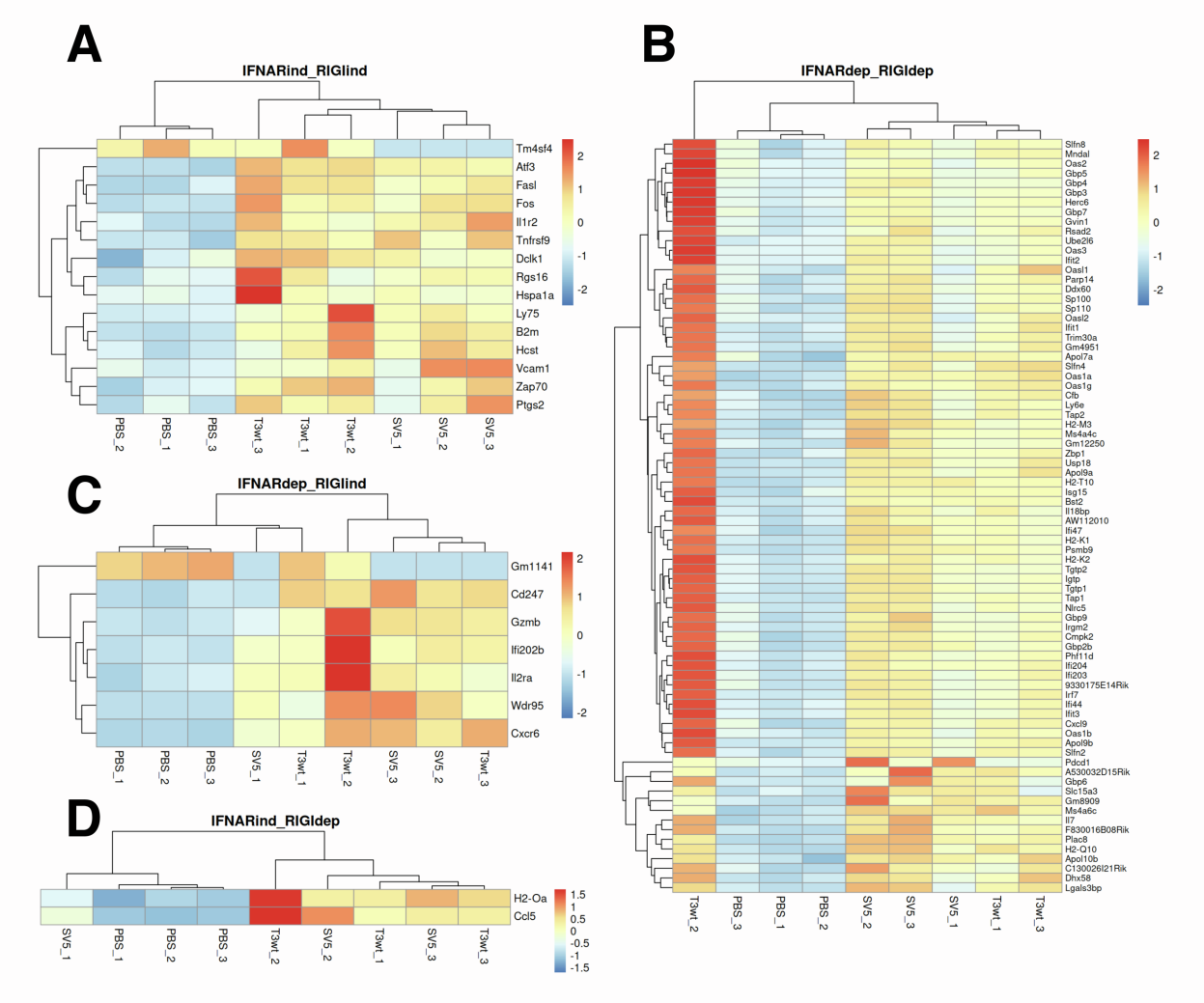

Figure S8: Differentially expressed genes from the IFN pathways among tumors after oncolytic treatments. Diagram of the animal experiment can be found in Figure 5A. TUBO cells were implanted into the mammary fat pad of BALB/c mice. When tumors were palpable, we performed three intratumoral injections (days 1, 3 and 5) with PBS or virus at 5 x 10^8 PFU/injection. At day 14 post virus injections mice were euthanized, and tumors were collected for RNA sequencing. **A.** Heat map showing differential expressed genes from the IFN-receptor independent and RIG-I independent pathway. **B.** Heat map showing differential expressed genes from the IFN-receptor dependent and RIG-I dependent pathway. **C.** Heat map showing differential expressed genes from the IFN-receptor dependent and RIG-I independent pathway. **D.** Heat map showing differential expressed genes from the IFN-receptor independent and RIG-I dependent pathway. Upregulated transcripts are shown in a red scale of colors and downregulated transcripts are shown in a blue scale of colors. Genes corresponding to the different pathways were obtained from Mohamed et. al. 2020 [4].

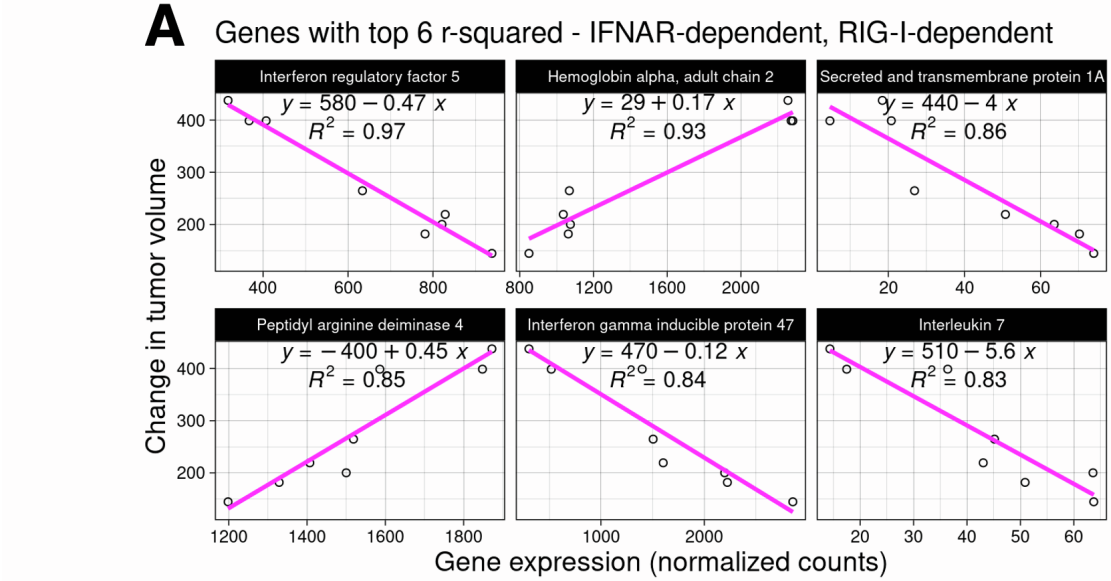
A
Genes with top 6 r-squared - IFNAR-dependent, RIG-I-dependent
Interferon regulatory factor 5
y = 580 − 0.47 x
R2 = 0.97
Hemoglobin alpha, adult chain 2
y = 29 + 0.17 x
R2 = 0.93
Secreted and transmembrane protein 1A
y = 440 − 4 x
R2 = 0.86
Peptidyl arginine deiminase 4
y = −400 + 0.45 x
R2 = 0.85
Interferon gamma inducible protein 47
y = 470 − 0.12 x
R2 = 0.84
Interleukin 7
y = 510 − 5.6 x
R2 = 0.83
Change in tumor volume
Gene expression (normalized counts)

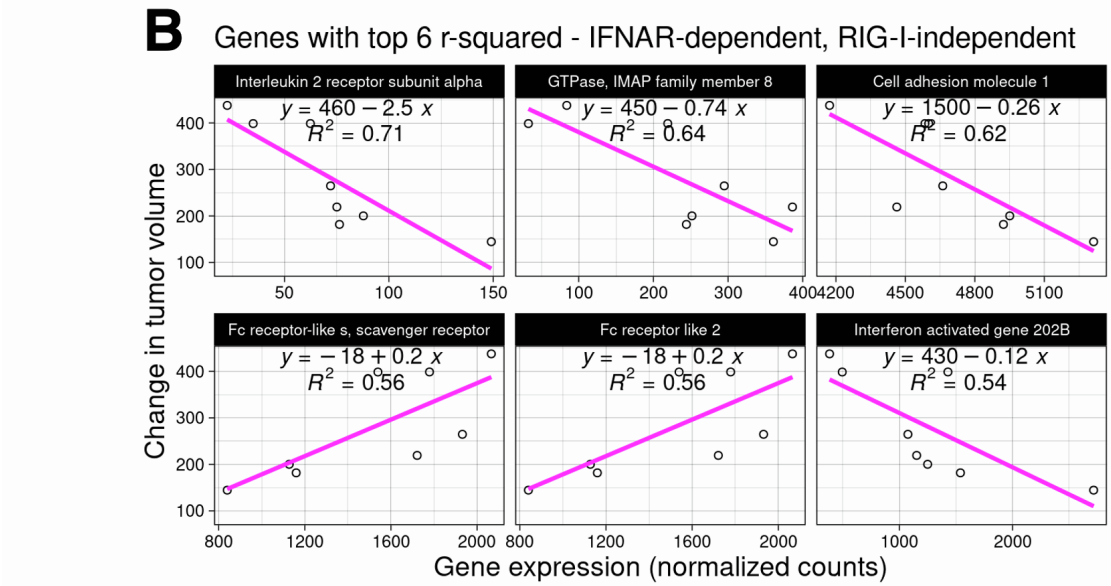
B
Genes with top 6 r-squared - IFNAR-dependent, RIG-I-independent
Interleukin 2 receptor subunit alpha
y = 460 − 2.5 x
R2 = 0.71
GTPase, IMAP family member 8
y = 450 − 0.74 x
R2 = 0.64
Cell adhesion molecule 1
y = 1500 − 0.26 x
R2 = 0.62
Fc receptor-like s, scavenger receptor
y = −18 + 0.2 x
R2 = 0.56
Fc receptor like 2
y = −18 + 0.2 x
R2 = 0.56
Interferon activated gene 202B
y = 430 − 0.12 x
R2 = 0.54
Change in tumor volume
Gene expression (normalized counts)

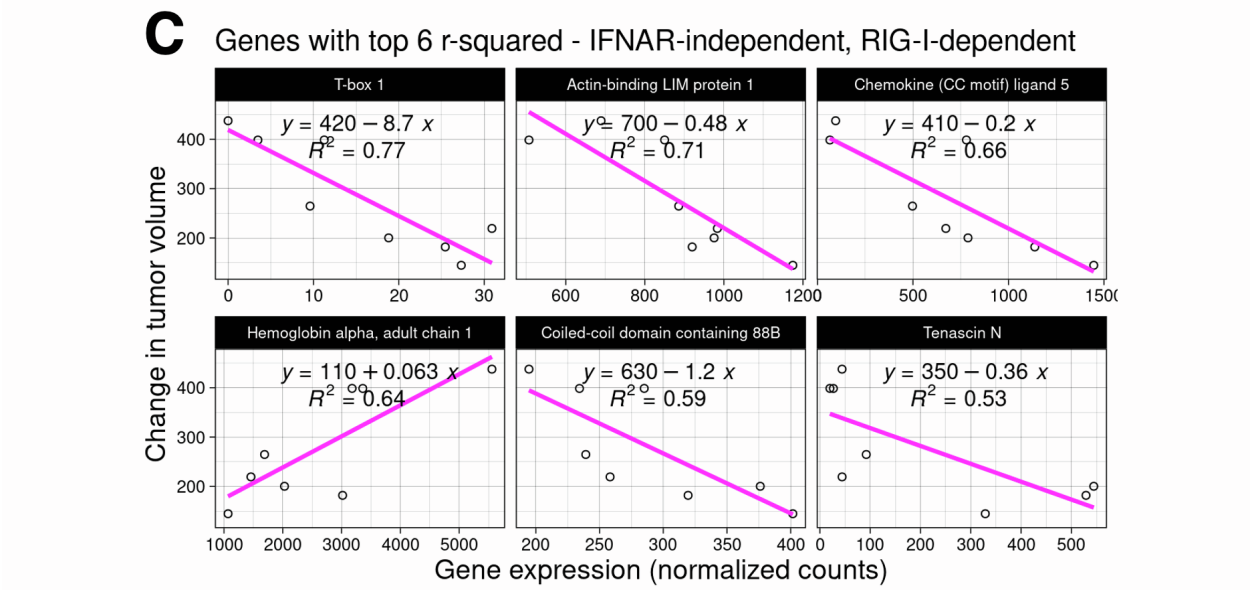

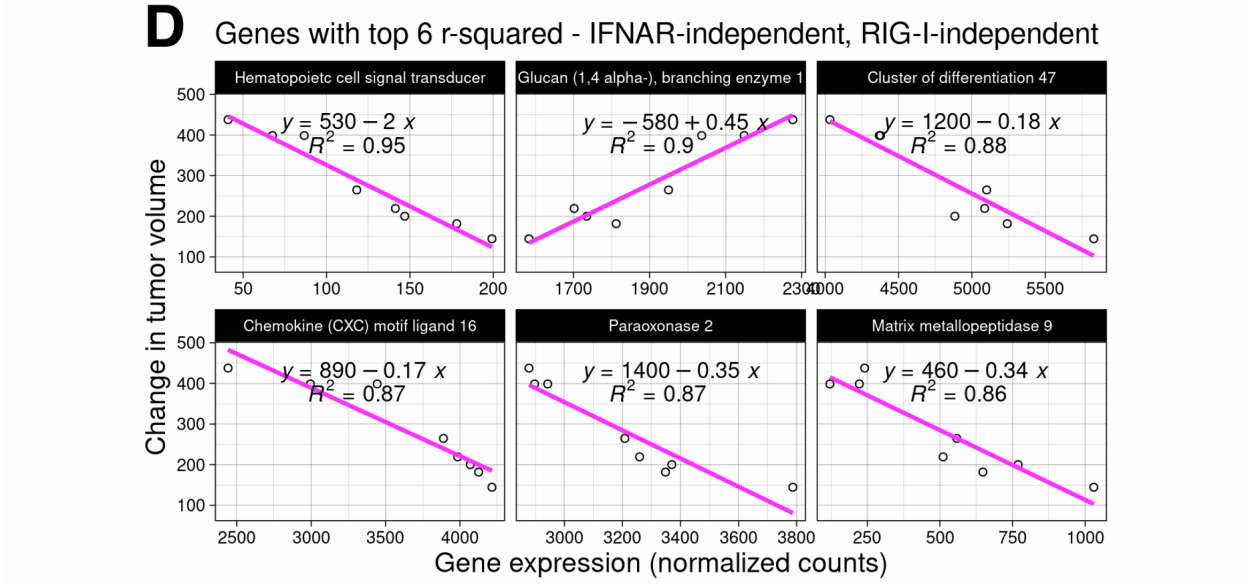

Figure S9: Top six correlations among expressed genes from the IFN pathways and tumor growth. According to the experiment diagram shown in Figure 5A, tumors were collected for RNA sequencing analyses. The correlations among genes associated with four distinct signaling pathways and changes in tumor volume, regardless of the administered treatments, were assessed. Here, we present the top six correlations from these analyses, categorized by the following signaling pathways: **A.** IFN-receptor dependent and RIG-I dependent pathway. **B.** IFN-receptor dependent and RIG-I independent pathway. **C.** IFN-receptor independent and RIG-I dependent pathway. **D.** IFN-receptor independent and RIG-I independent pathway. Genes corresponding to the different pathways were obtained from Mohamed et. al. 2020 [4]. The rest of the genes and their correlation with change in tumor volume can be found in the **Table S6.**

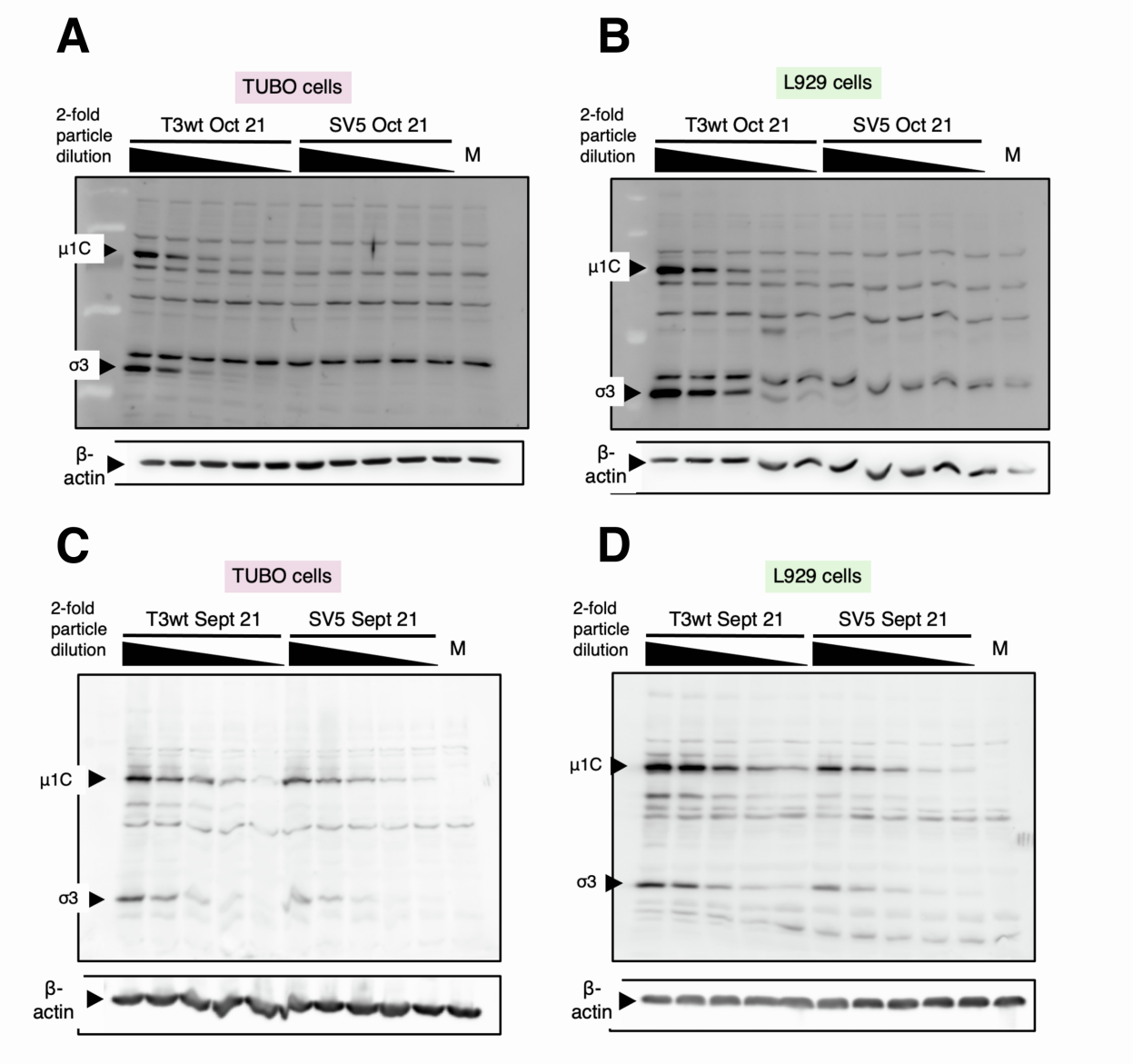

Figure S10: SV5 exhibits lower binding efficiency to TUBO cells compared to T3wt. The same number of T3wt or SV5 (stocks October 2021 and September 2021) virus particles were 2-fold serially diluted and added to TUBO or L929 cells. A binding assay with subsequent Western blot was performed. The polyclonal anti-reovirus antibody was used to evaluate the presence of the structural reovirus proteins µ1C and σ3. The intensity of the bands at the same number of particles was compared between viruses as an indication of the level of virus particles bound to the cells. **A.** Binding of October 2021 viruses to TUBO cells. **B.** Binding of October 2021 viruses to L929 cells. **C.** Binding of September 2021 viruses to TUBO cells. **D.** Binding of September 2021 viruses to L929 cells.

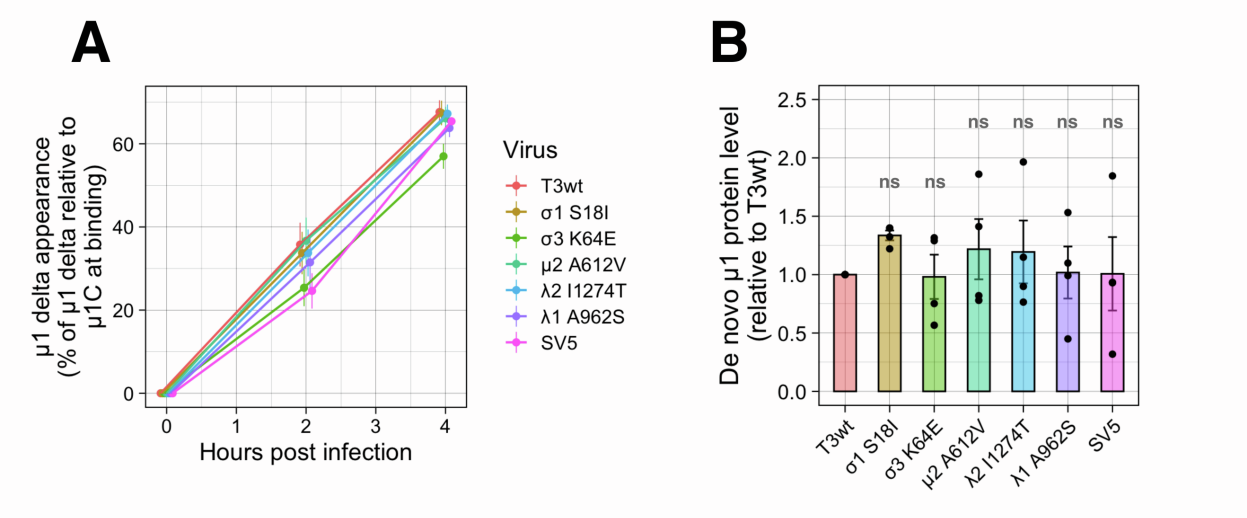

Figure S11: SV5 uncoats and produces viral proteins at a similar rate as T3wt. A. Virus uncoating represented by the appearance of the δ fragment (cleaved μ1C) of T3wt, SV5 and single-mutated viruses in L929 cells at 2 and 4 hpi by Western blot analyses (n = 3). **B.** *De novo* μ1 protein production (representative of viral protein synthesis) at 6 hpi with T3wt, SV5 or single-mutated viruses in L929 cells (n = 3). For virus uncoating and *de novo* protein production, Western blot analysis was performed with a polyclonal anti-reovirus antibody. Virus protein production in T3wt-infected cells was set arbitrarily to 1.0. ns: non-significant (ANOVA with Tukey test).

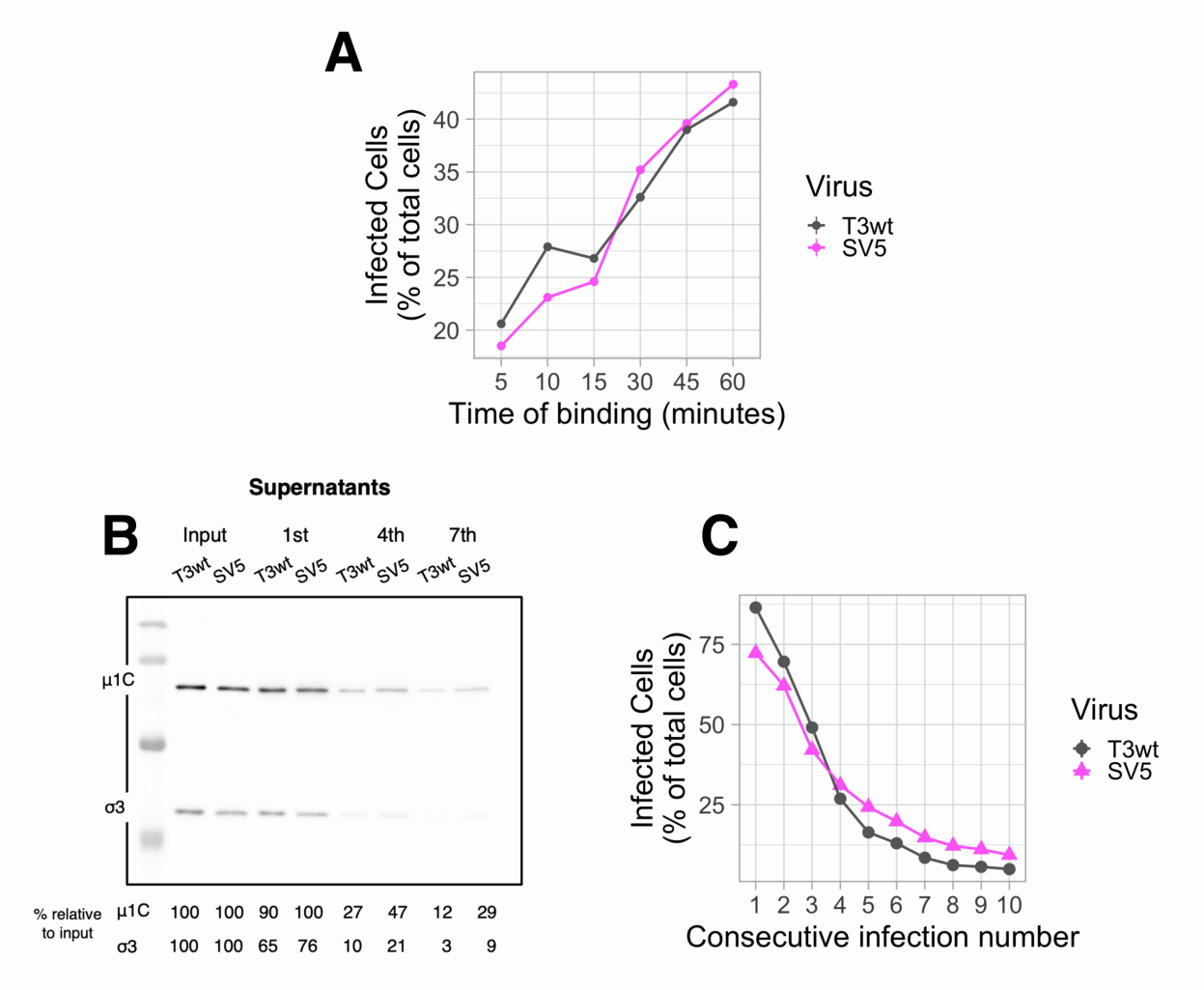

Figure S12: Consecutive binding experiment optimization. **A.** Optimization of time of binding (n = 1). The time of binding was optimized to give significant binding to L929 cells at each of the 10 rounds of consecutive infections without exhausting the amount of virus before the end of the experiment. Infected cells were determined by flow cytometry with the monoclonal antibody anti-µ1 (10F6). **B**. Increased SV5 presence in supernatants in the 4th and 7th infections in the consecutive-infection experiment (n = 1). To corroborate that the limited SV5 binding was increasing the amount of virus particles in the supernatants, we decided to collect some supernatants during one of the consecutive experiments (Shown in C). Supernatants were subjected to Western blot analysis with a polyclonal anti-reovirus antibody to determine the levels of outer capsid viral proteins. **C.** Graph showing infected cells determined by flow cytometry with the monoclonal antibody anti-µ1 (10F6) during each consecutive infection.

Table S1: Mutations in isolated reovirus variants. Table depicts original isolated reovirus variant, mutated viral gene, position and description of mutated nucleotide, and position and description of mutated amino acid.

Original reovirus variant	Mutated gene	Nucleotide mutation	Mutated protein	Amino acid change
T3v2, T3v12	S1	G-65-T	σ1	S-18-I
T3v16	S1	T-95-C	σ1	L-28-P
T3v8	S1	G-209-T	σ1	S-66-I
T3v13	S1	A-352-C	σ1	T-114-P
T3v6	S1	G-663-T	σ1	Q-217-H
T3v13	S1	G-668-A	σ1	R-219-Q
T3v16	S1	T-95-C	σ1	L-28-P
T3v12	S4	A-222-G	σ3	K-64-E
T3v4	S4	T-722-G	σ3	H-230-Q
T3MB-2	M2	G-709-C	μ1	S-227-T
T3v6	M1	C-347-T	μ2	L-112-F
T3v10	M1	C-1848-T	μ2	A-612-V
T3v6	M1	T-1850-G	μ2	S-613-A
T3v12	L3	T-377-C	λ1	Y-122-H
T3v1	L3	A-425-G	λ1	N-138-D
T3v11	L3	G-2897-T	λ1	A-962-S
T3v6	L2	G-1235-A	λ2	D-408-N
T3v1	L2	G-3316-A	λ2	M-1101-I
T3v14	L2	A-3456-G	λ2	N-1148-S
T3v4	L2	A-3835-G	λ2	I-1274-M

Original reovirus variant	Mutated gene	Nucleotide mutation	Mutated protein	Amino acid change
T3v5	L2	T-3834-C	λ2	I-1274-T
T3v1	L1	C-1216-T	λ3	P-400-S
T3v4	L1	G-2694-A	λ3	M-892-I
T3v12	L1	A-2933-G	λ3	Q-972-R

Table S2: Primers used for site directed mutagenesis

Mutated gene	Nucleotide mutation	Primers*
S1	G-663-T	5'-ggaattgatcagtattaaatcgaaaAtgaagtccaccattttgaatattca-3' 3'-ccttaactagtcataatttagctttTacttcaggtggtaaaacttataagt-5'
S1	G-209-T	5'-aagtcatcccgaAtttgctcaagagcgatgattcgt-3' 3'-ttcagtagggctTaaacgagttctcgctactaagca-5'
S1	A-946-G	5'-ctctgcctaaacctataaTctggactcattccgataccg-3' 3'-gagacggatttggatattAaacctgagtaaggctatggc-5'
S1	G-65-T	5'-cggctgataatcgcattaacgaTtgataatggagcatca-3' 3'-gccgactattagcgtaattgctAactattacctcgtagt-5'
S1	A-352-C	5'-gctctgcaagtcctgGctcaagttgtcccac-3' 3'-cgagacgttcaggacCgagttcaacagggtg-5'
S1	G-668-A	5'-tctggaattgatcagtattaaatTgaaactgaagtccaccattttg-3' 3'-agaccttaactagtcataatttaActttgacttcaggtggtaaaac-5'
S1	T-95-C	5'-ccgagacccttgattcaGgccctttgacagtgat-3' 3'-ggctctgggaactaagtCcgggaaaactgtcacta-5'
S4	A-222-G	5'-aggcaaatgcttcagctCgcgttgtagagatccaa-3' 3'-tccgtttacgaagtcgaGcgcaacatctctaggtt-5'
S4	T-722-G	5'-gcccttcgatggatcCtgatccagctcagag-3' 3'-cgggaagctacctagGactaggtcgagtctc-5'
M1	C-347-T	5'-tcatcatctttcctgaAatctttctttagcattagtcgtttacgaag-3' 3'-agtagtagaaaggactTtagaaagaaatcgtaatcagcaaatgcttc-5'
M1	T-1850-G	5'-cagccgacgtagCtgccgggtctgc-3' 3'-gtcggctgcatcGacggcccagacg-5'
M1	C-1848-T	5'-cagccgacgtagatAccgggtctgcttct-3' 3'-gtcggctgcatctaTggcccagacgaaga-5'
M2	G-709-C	5'-ctccgtatcaggGtgtcatctggcagctgat-3' 3'-gaggcatagtccCacagtagaccgtcgacta-5'
L2	A-3835-G	5'-acaatgtatgtgggCatcgatggggaccaacttatg-3' 3'-tgttacatacacccGtagctacccctggttgaatac-5'
L2	T-3834-C	5'-aatgtatgtgggtGtcgatggggaccaacttatgg-3' 3'-ttacatacacccaCagctacccctggttgaatacc-5'
L2	G-1235-A	5'-cagatcgccttcgtTcatcgctgcctggt-3' 3'-gtctagcggaagcaAgtagcgacggacca-5'
L2	A-3456-G	5'-cgggaactgatgtcgatataacagttaGtccttattaccgtc-3' 3'-gcccttgactacagctatattgtcaatCaggaataatggcag-5'

Mutated gene	Nucleotide mutation	Primers*
L2	G-3316-A	5'-cactagagcctg**T**atggtatagattcctgcgtcgg-3' 3'-gtgatctcggac**A**taccatatctaaggacgcagcc-5'
L3	G-2897-T	5'-caaatgtcgccg**A**cgtcgccgccga-3' 3'-gtttacagcggc**T**gcagcggcggct-5'
L3	T-377-C	5'-ttattgataccagtgtctgaat**G**tgtgacttgcgctttacttttg-3' 3'-aataactatggtcacagactta**C**acactgaacgcgaaatgaaaac-5'
L3	A-425-G	5'-caccctcattatccacat**C**ccagatcttgacagttc-3' 3'-gtgggagtaataggtgta**G**ggtctagaactgtcaag-5'
L1	G-2694-A	5'-cccagatctccagtagg**T**atgtaccaagaaaatatccatg-3' 3'-gggtctagaggtcatcc**A**tacatggttcttttataggtac-5'
L1	A-2933-G	5'-gtagatagtcggataatgcc**C**gagtgaattgttctcttacc-3' 3'-catctatcagcctattacgg**G**ctcacttaacaagagaatgg-5'
L1	C-1216-T	5'-agtctttctggg**A**aatgggaaccttaatctccggac-3' 3'-tcagaaagaccc**T**ttacccttggaattagaggcctg-5'

*Red and uppercase letters indicate the location of the mutation in the primers.

Table S3: Antibodies used to determine frequency of T cells

Antibody	Catalog number	Company
CD45-FITC	103108	BioLegend
Tetramer (H-2K(d)-TYVPANASL) PE	---	NIH
CD3-PECy7	100220	BioLegend
CD4-APC	116014	BioLegend
CD8a-Brilliant Violet 421	100738	BioLegend
CD19-APC Fire 750	115558	BioLegend
CD25-PE/Dazzlet™594	102048	BioLegend
Zombie Aqua	423102	BioLegend

Table S4: Antibodies used to determine frequency of innate immune cells

Antibody	Catalog number	Company
CD45-FITC	103108	BioLegend
CD3-PECy7	100220	BioLegend
CD11b-PE	101208	BioLegend
Ly6G/Ly6C (Gr-1)	108434	BioLegend
CD11c-APC Fire 750	117352	BioLegend
F4/80-PerCP-Cy5.5	123128	BioLegend
CD49b pan-NK cells APC	108910	BioLegend
Zombie Aqua	423102	BioLegend

Table S5: Excel spreadsheet displaying the list of signatures genes used as transcriptomic markers in the murine Microenvironment Cell-populations-counter (mMCP-counter) analysis.

Table S6: Excel spreadsheet showing the rest of the correlations (non-top six) between change in tumor volume and IFN-pathways genes.

References

(1) Sturm, G.; Finotello, F.; List, M. Immunedeconv: An R Package for Unified Access to Computational Methods for Estimating Immune Cell Fractions from Bulk RNA-Sequencing Data. *Methods Mol Biol* **2020**, *2120*, 223-232. DOI: 10.1007/978-1-0716-0327-7_16.

(2) Sturm, G.; Finotello, F.; Petitprez, F.; Zhang, J. D.; Baumbach, J.; Fridman, W. H.; List, M.; Aneichyk, T. Comprehensive evaluation of transcriptome-based cell-type quantification methods for immuno-oncology. *Bioinformatics* **2019**, *35* (14), i436-i445. DOI: 10.1093/bioinformatics/btz363.

(3) Petitprez, F.; Levy, S.; Sun, C. M.; Meylan, M.; Linhard, C.; Becht, E.; Elarouci, N.; Tavel, D.; Roumenina, L. T.; Ayadi, M.; et al. The murine Microenvironment Cell Population counter method to estimate abundance of tissue-infiltrating immune and stromal cell populations in murine samples using gene expression. *Genome Med* **2020**, *12* (1), 86. DOI: 10.1186/s13073-020-00783-w.

(4) Mohamed, A.; Konda, P.; Eaton, H. E.; Gujar, S.; Smiley, J. R.; Shmulevitz, M. Closely related reovirus lab strains induce opposite expression of RIG-I/IFN-dependent versus -independent host genes, via mechanisms of slow replication versus polymorphisms in dsRNA binding sigma3 respectively. *PLoS Pathog* **2020**, *16* (9), e1008803. DOI: 10.1371/journal.ppat.1008803.